PCCP

Cite this: *Phys. Chem. Chem. Phys.*, 2012, **14**, 14270–14276

www.rsc.org/pccp

PAPER

Yield of exciton dissociation in a donor–acceptor photovoltaic junction†

Guangqi Li,[a] Abraham Nitzan[b] and Mark A. Ratner*[ac]

Received 12th May 2012, Accepted 9th August 2012
DOI: 10.1039/c2cp41532a

A simple model is constructed to describe dissociation of charge transfer excitons in bulk heterojunction solar cells, and its dependence on the physical parameters of the system. In bulk heterojunction organic photovoltaics (OPVs), exciton dissociation occurs almost exclusively at the interface between the donor and acceptor, following one-electron initial excitation from the HOMO to the LUMO levels of the donor, and charge transfer to the acceptor to make a charge-transfer exciton. After exciton breakup, and neglecting the trapping of individual carriers, the electron may undergo two processes for decay: one process involves the electron and/or hole leaving the interface, and migrating to the electrode. This is treated here as the electron moving on a set of acceptor sites. The second loss process is radiationless decay following recombination of the acceptor electron with the donor cation; this is treated by adding a relaxation term. These two processes compete with one another. We model both the exciton breakup and the subsequent electron motion. Results depend on tunneling amplitude, energetics, disorder, Coulomb barriers, and energy level matchups, particularly the so-called LUMO–LUMO offset.

I. Introduction

Organic photovoltaics (OPVs)[1–12] are both fascinating from a fundamental point of view, and promising as a major response to the challenge of green energy capture.[13] The most common approach to OPVs is the bulk heterojunction (BHJ) cell, which consists of mixed donor (D) and acceptor (A) species that form interpenetrating connective networks.[14–22] In such OPVs, a major problem occurs that is absent in traditional semiconductor photovoltaics (because of band bending in those situations).[23] This issue involves the efficiency of charge separation following photoexcitation. Coulomb attraction between electrons and holes (located on the A and D species respectively) can cause the exciton to remain stuck at the interface,[24–26] where it can undergo nonradiative decay, substantially reducing the efficiency.

Here we use a very simple model both to analyze some aspects of this issue of exciton breakup and to examine the dependence on the physical parameters of the system. We model the motion only of the electron (although the hole behavior is similar). We treat each A molecule as a single level (corresponding to the LUMO in simplified one-electron language, for each A site). The sites are taken as degenerate, in a linear array. The initial state is formed by excitation of the D, followed by electron transfer to form the exciton at the interface by occupying the A site on the first A molecule in the chain, leaving a hole on D. We follow the dynamics using a density matrix approach.

The Hamiltonian includes the energy levels of the D and A sites, the Coulomb interaction between the electron and the hole, and the motion along the A chain. Added to the Hamiltonian are a self-energy term describing the injection of the electron into the electrode,[27–31] and first order relaxation caused by nonradiative decay of the charge transfer exciton back to the ground state of the system.[32]

We find that the yield depends upon relationships between the band width and the so-called LUMO–LUMO gap (this linguistic shorthand is the energetic difference between the photoexcited donor and the D^+A^- charge transfer exciton). When this LUMO–LUMO gap is either too small or too large, motion is impeded: if it is too large, the narrow transport band of the acceptor cannot accommodate the energy, and therefore the exciton does not separate. When it is too small, it cannot overcome the Coulomb trapping (at least within the current model that does not include vibrational relaxation times). Suggestions are made for optimization of actual cells.

II. Theoretical model

Fig. 1 sketches the very simple model, consisting of a zeroth site corresponding to the excited donor, and sites 1 through N, corresponding to the anion formed after charge transfer from

[a] *Non-equilibrium Energy Research Center (NERC), Northwestern University, Evanston 60208, USA. E-mail: ratner@northwestern.edu*
[b] *Raymond and Beverly Sackler Faculty of Exact Sciences, School of Chemistry, Tel-Aviv University, Tel-Aviv 69978, Israel*
[c] *Department of Chemistry, Northwestern University, Evanston 60208, USA*

† Electronic supplementary information (ESI) available. See DOI: 10.1039/c2cp41532a

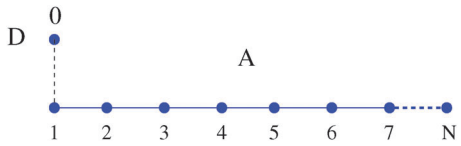

Fig. 1 The scheme of a donor–acceptor system. Donor part D including single site 0 and acceptor part A including the sites from 1 to N. The sites to the right of N will be treated as generating a self-energy.

the donor to the acceptor at the interface. The sites beyond N will be represented by a complex valued self-energy term added to the energy associated with site N. The one-electron Hamiltonian is simply

$$H_S = \varepsilon_0 c_0^\dagger c_0 + 2b\sum_{l=1}^{N} c_l^\dagger c_l + m(c_0^\dagger c_1 + c_1^\dagger c_0) + b\sum_{l=1}^{N-1}(c_l^\dagger c_{l+1} + c_{l+1}^\dagger c_l), \quad (1)$$

where the operators $c_l^\dagger(c_l)$ create (annihilate) an electron in site l. ε_0 is the energy level of site 0, $2b$ ($b > 0$) is the energy level of the other sites. We take the intersite coupling on the acceptor chain to be b, effectively setting the bottom of the A band to be 0. In the picture the LUMO–LUMO gap may be associated with the distance $|\varepsilon_0 - 2b|$ to the band center, or with ε_0 – the distance to the band bottom.

III. Self-energy

Our full system includes a semi-infinite chain of A sites. It is convenient to represent it by a finite N-site system where the effect of the rest of the A chain is taken into account by adjusting the energy of site N by a self-energy term[27,28,33]

$$\sum(E) = \frac{E - 2b - \sqrt{(E-2b)^2 - 4b^2}}{2}, \quad (2)$$

where E is the injected energy. If E is in the energy band, *i.e.*, $0 \le E \le 4b$, $\Sigma(E)$ will be

$$\sum(E) = \frac{E - 2b - i\sqrt{4b^2 - (E-2b)^2}}{2} = \Lambda(E) - \frac{i}{2}\Gamma(E), \quad (3)$$

with $\Lambda(E) = \frac{E-2b}{2}$ and $\Gamma(E) = \sqrt{4b^2 - (E-2b)^2}$ being real numbers. In the simplest approximation we can replace the self-energy by its average over the band

$$\chi = \frac{1}{C}\int_{E=0}^{E=4b} \mathrm{d}E\Lambda(E) - \frac{i}{2C}\int_{E=0}^{E=4b} \mathrm{d}E\Gamma(E) \quad (4)$$

with $C = \int_{E=0}^{E=4b} \mathrm{d}E$. The first term on the right side of formula (4) is 0, and the second term is a negative imaginary number. Then we get $\chi = -i\frac{|b|\pi}{4}$ and the Hamiltonian of this contribution part working as a sink can be expressed as

$$H_{\mathrm{sink}} = \chi c_N^\dagger c_N = -i\frac{|b|\pi}{4} c_N^\dagger c_N. \quad (5)$$

IV. Coulomb interaction

To account for coulomb interaction between the moving electron and the hole left behind we also add a charge-trapping term to the system Hamiltonian as

$$H_{\mathrm{cou}} = -V\sum_{l=1}^{N}\frac{1}{\varepsilon r_l} c_l^\dagger c_l, \quad (6)$$

where V is the parameter describing the attraction to the hole at site 0, $r_l = l\alpha$ is the distance between site 0 and l with α being the lattice distance and ε being the dielectric constant. By denoting $\gamma = \frac{V}{\varepsilon\alpha}$ eqn (6) takes the form

$$H_{\mathrm{cou}} = -\gamma\sum_{l=1}^{N}\frac{1}{l} c_l^\dagger c_l. \quad (7)$$

V. Time evolution and exciton recombination

Up to now, the effective system Hamiltonian H_{eff} can be expressed as

$$H_{\mathrm{eff}} = H_S + H_{\mathrm{sink}} + H_{\mathrm{cou}}, \quad (8)$$

and the time-evolution of the density matrix ρ of this $N + 1$ site system can be expressed by the Liouville equation as

$$i\hbar\frac{\mathrm{d}\rho}{\mathrm{d}t} = [H_{\mathrm{eff}}, \rho] = H_{\mathrm{eff}}\rho - \rho H_{\mathrm{eff}}^+, \quad (9)$$

which will be solved by using the Runge–Kutta method with the initial condition that there is one electron on the donor site 0. $H_{\mathrm{eff}}{}^+$ is a conjugate transpose of H_{eff} because of the complex diagonal elements in eqn (5).

Exciton recombination is a relaxation process that reduces the probability of charge separation. To take this process into account we assume that the initial state on site 0 has a finite relaxation rate η. In the associated Liouville equations this relaxation affects the time evolution of ρ_{00} and of all non-diagonal elements ρ_{0j} and ρ_{j0}, according to

$$i\hbar\frac{\mathrm{d}\rho_{0,0}}{\mathrm{d}t} = [H_{\mathrm{eff}}, \rho]_{0,0} - \eta\rho_{0,0}, \quad (10)$$

$$i\hbar\frac{\mathrm{d}\rho_{0,j}}{\mathrm{d}t} = [H_{\mathrm{eff}}, \rho]_{0,j} - \frac{\eta}{2}\rho_{0,j}, \quad \text{for } j \neq 0, \quad (11)$$

$$i\hbar\frac{\mathrm{d}\rho_{j,0}}{\mathrm{d}t} = [H_{\mathrm{eff}}, \rho]_{j,0} - \frac{\eta}{2}\rho_{j,0}, \quad \text{for } j \neq 0. \quad (12)$$

VI. Yield of charge separation

Since the sites beyond N work as sinks absorbing the population at site N, the yield Y of charge separation can be obtained by

$$Y = \frac{2i\chi}{\hbar}\int_0^\infty \mathrm{d}t\rho_{NN}(t), \quad (13)$$

where $\rho_{NN}(t)$ is the population on the site N which changes with time and is absorbed by the sink. So the integral of the ρ_{NN} over time should be the total population absorbed by the sink, *i.e.*, the yield. We will calculate the yield of charge

separation as a function of donor state energy ε_0, the coulomb attraction γ, the acceptor band width 4b and the decay parameter η.

The total population distribution P_O on the active sites is

$$P_O = \sum_{l=0}^{N} \langle c_l^\dagger c_l \rangle. \quad (14)$$

For $\eta = 0$, *i.e.*, without the population decay process inside the donor, $1 - P_O$ should be the population absorbed by the sink, equal to the yield. When $\eta \neq 0$, $1 - P_O$ should be larger than the yield since some population decays through the donor.

VII. Numerical results

A. Energy gap and charge transfer rate effects

For the numerical simulation, we use $b = 0.2$ eV, $N = 60$ and we change energy level ε_0, charge trapping parameter γ, decay parameter η and coupling parameter m. We also examine a situation with random disorder, by taking random energies ε_r for the acceptor energy levels and random parameters b_r for the coupling between acceptor neighbor sites, to see the influence on the population distribution along the chain and on yield of charge separation.

For an isolated system only including acceptor energy levels with $\gamma = 0$, the energy band is in the energy region $[0, 4b]$ with a band width $4b$. After switching on the coupling parameter m between site 0 and site 1, the effective acceptor bandwidth becomes narrower.

Such a D–A system can be taken as the single D site coupling to a energy band, obtained by diagonalizing the Hamiltonian of an isolated system including the A part. For a large N there will be enough eigenvalues inside the band to effectively link to the active site over the relevant energy range. In the supplementary information†, Fig. S3 shows the dependence of the yield on the site number N. When N exceeds 16, the band widths effectively remain constant.

B. Effects of coulomb trapping

In Fig. 2 and 3 the long time yield Y and the total population P_O left on the chain are shown as a function of ε_0, changing with the coupling parameter m and the charge trapping parameter γ. With $\eta = 0$ all the population can only decay through the first process. The yield Y is then exactly $1 - P_O$.

Fig. 2 shows the dependence of yield Y on m. With the energy gap ε_0 inside the band, *i.e.*, $0 \leq \varepsilon_0 \leq 4b$, the yield remains 1 for the energy around the middle point $\varepsilon_0 = 2b = 0.4$ eV. For $\varepsilon_0 \ll 2b$ or $\varepsilon_0 \gg 2b$ the yield decreases with increasing m and the yield curve broadens. For the energy gap ε_0 outside the band, most populations will stay on the chain because they are localized by an energy blockade phenomenon (they lie too high in energy to decay into the band). However the population can still decay to the electrode through channels with a relatively large imaginary part and induce a very small yield. With a large m, more population can tunnel through the acceptor sites migrating to the electrode with the yield increasing.

The effect of the charge trapping γ is to down shift the energy levels of the acceptor sites and therefore the band. As shown in Fig. 3 the line shape just moves to its left slightly, broadens only slightly, and becomes asymmetric because the shift reduces the energy gap between the donor and acceptor sites. The effect of γ is small because there is no competition from nonradiative decay.

C. Nonradiative decay effects

Upon switching on the nonradiative decay process ($\eta \neq 0$), for "LUMO–LUMO gap" ε_0 outside the band, the localized

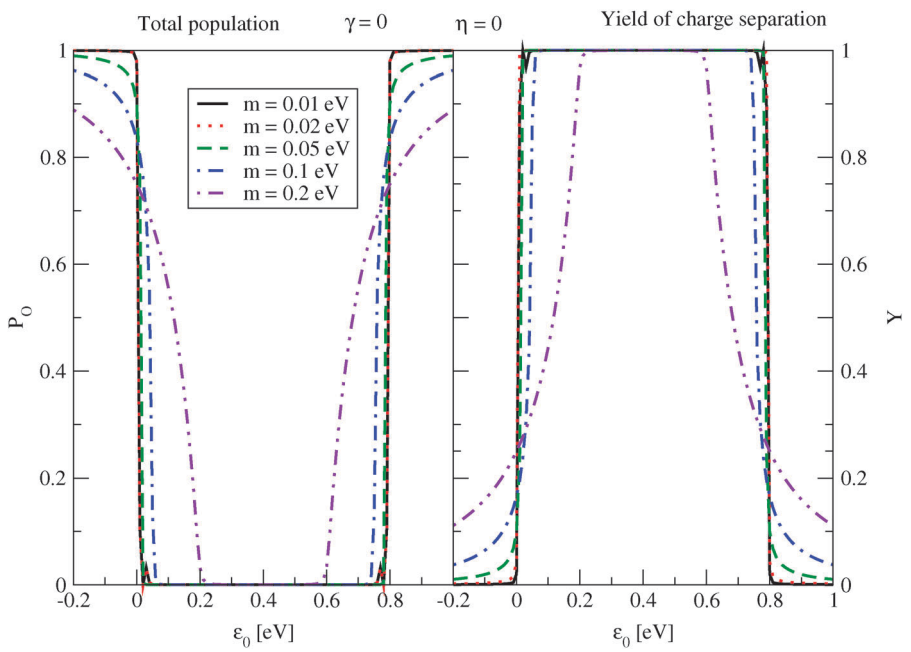

Fig. 2 Population P_O (left panel) and yield Y of charge separation (right panel) as a function of ε_0 obtained with different coupling parameter m. $N = 60$, $b = 0.2$ eV, decay parameter $\eta = 0$ and charge trapping parameter $\gamma = 0$. $m = 0.01$ eV (black line); $m = 0.02$ eV (dotted line); $m = 0.05$ eV (dashed line); $m = 0.1$ eV (dotted + dashed) and $m = 0.2$ eV (double dotted + dashed).

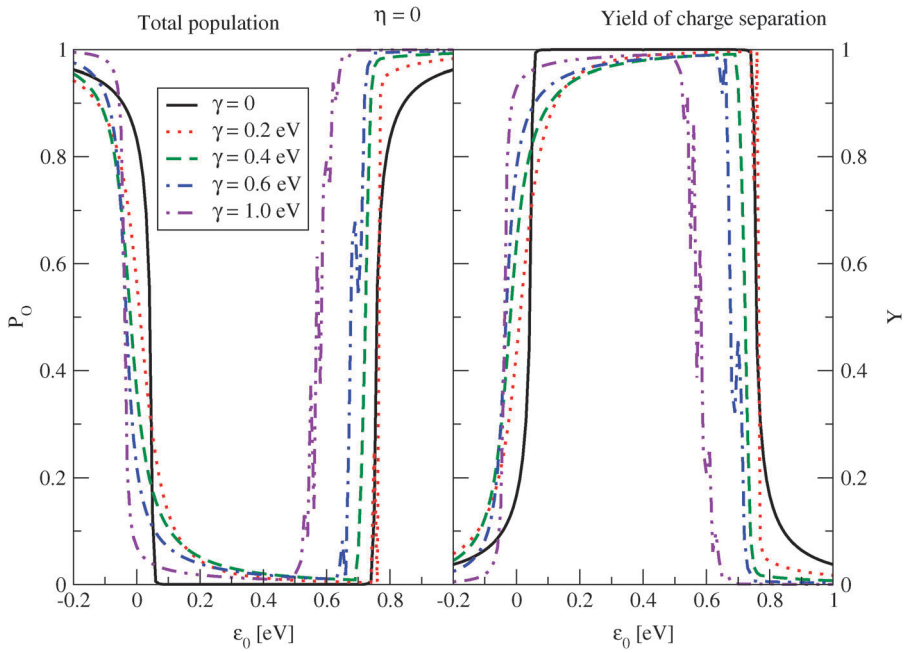

Fig. 3 Population P_O (left panel) and yield Y of charge separation (right panel) as a function of ε_0 obtained with different charge trapping parameter γ. $N = 60$, $b = 0.2$ eV, $m = 0.1$ eV, decay parameter $\eta = 0$. $\gamma = 0$ (black line); $\gamma = 0.2$ eV (dotted line); $\gamma = 0.4$ eV (dashed line); $\gamma = 0.6$ eV (dotted + dashed) and $\gamma = 1.0$ eV (double dotted + dashed).

population that cannot decay into the electrode through the first process will decay through the second process, and for long time no population remains on the chain. For gap ε_0 inside the band, the two decay processes will compete, reducing the yield. In Fig. 4 we examine the yield dependence on the decay parameter η and the coupling parameter m. With $\eta = 0$ the yield Y equals 1 for the energy inside the band. With increasing η, less population will exit through the electrodes, so the yield will decrease. Upon increasing m, more population will transfer from D to A, and eventually decay through site N, so yield increases with m.

Fig. 5 examines the effect of coulomb trapping. The line shape shows a loss of symmetry, as seen in Fig. 3. Even for small gap ε_0, the yield becomes small due to coulomb trapping. Here, the charge moves more slowly towards the electrode because of coulomb attraction to the hole, and so the

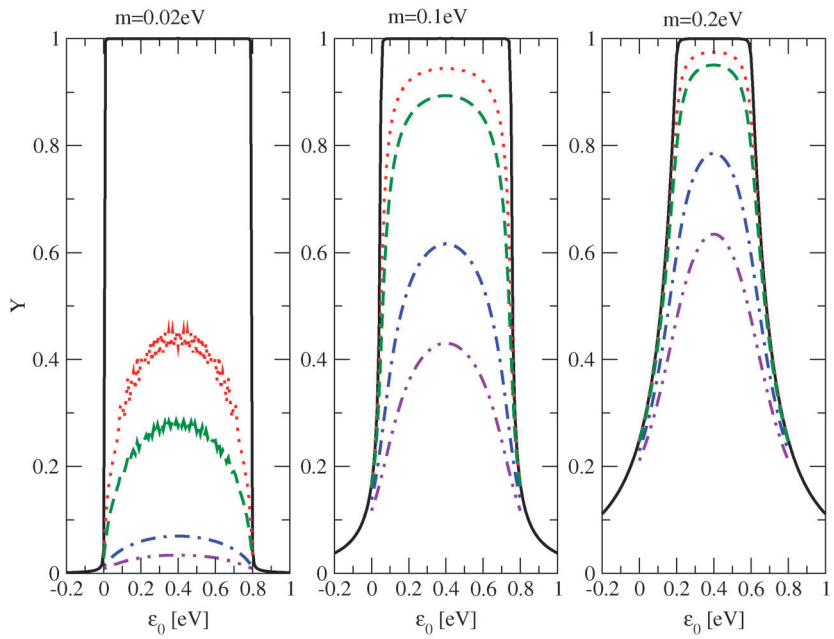

Fig. 4 Yield Y of charge separation as a function of ε_0 obtained with different decay parameter η and coupling parameter m. $N = 60$, $\gamma = 0$, $b = 0.2$ eV, $\eta = 0$ (black line); $\eta = 0.005$ eV (dotted line); $\eta = 0.01$ eV (dashed line); $\eta = 0.05$ eV (dotted + dashed) and $\eta = 0.1$ eV (double dotted + dashed), $m = 0.02$ eV (left panel); $m = 0.1$ eV (middle panel) and $m = 0.2$ eV (right panel).

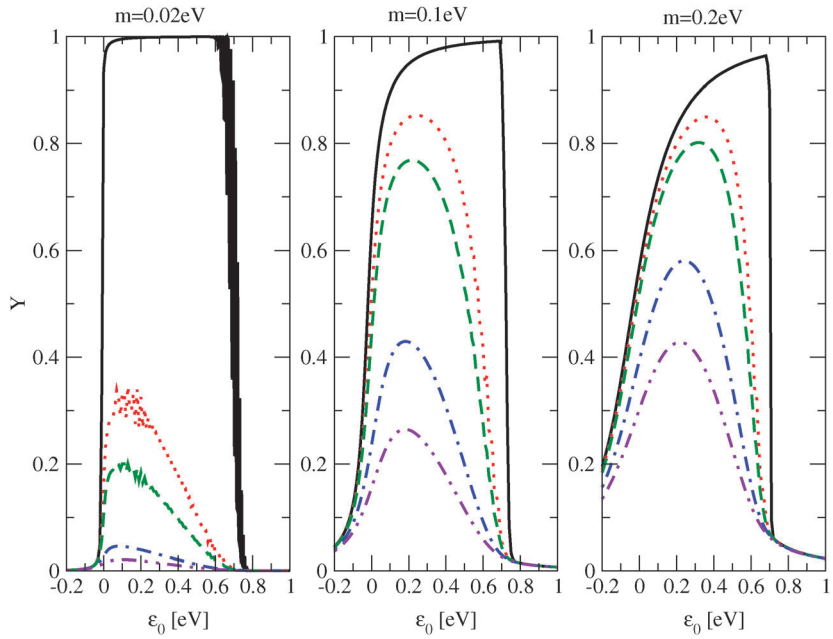

Fig. 5 Same as Fig. 4 but with $\gamma = 0.4$ eV. Because of a very long time decay process, the calculation was cut off at time $t = 32\,500$ fs, and line shape for $\eta = 0$ (black line) in the left panel shows oscillatory behavior.

nonradiative recombination can more easily destroy the exciton by recombination.

D. Structural randomness effects

Because of the random geometry in BHJ cells we expect intersite tunneling and site energies to vary randomly. To account for such structural randomness we have imposed random site-energies and intersite coupling elements on a finite section of our tight binding chain. The range beyond this section, that is part of the absorbing electrode, remains ordered. In Fig. 6 and 7 we examine the yield modifications by taking 30 random energy levels ε_r for the acceptor sites (from site 16 to site 45) and 29 random couplings b_r between these sites. In Fig. 6 we use random numbers for the 30 site energies and fix the energy levels of the others. In Fig. 7 we use 29 random numbers for the coupling elements. For each one, we average over 20 realizations. In each figure we choose a uniform random number distribution with differing widths.

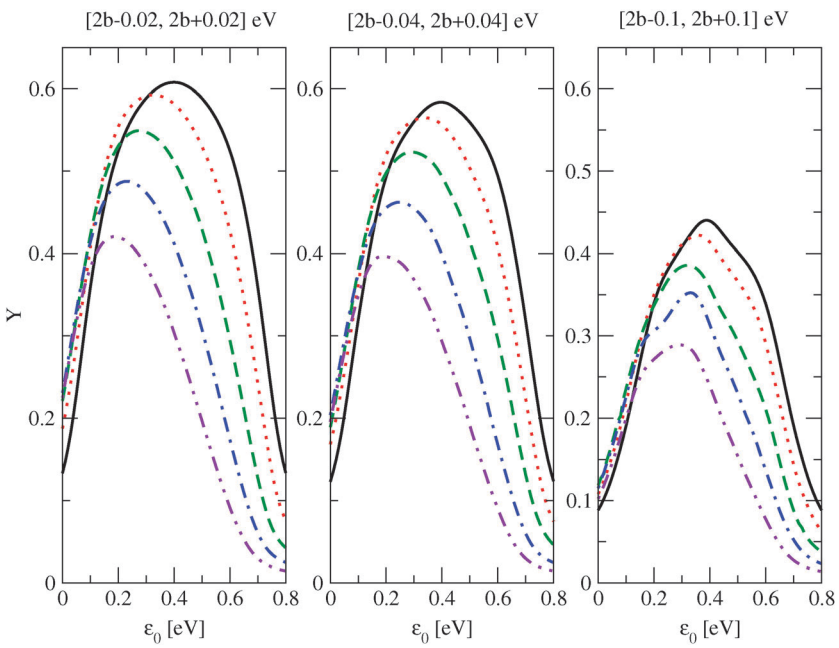

Fig. 6 Yield Y of charge separation as a function of ε_0 obtained with different γ and random energies ε_r for the 30 acceptor sites (from site 16 to site 45). $N = 60$, $\eta = 0.05$ eV, $b = 0.2$ eV, $m = 0.1$ eV. $\gamma = 0$ (black line); $\gamma = 0.1$ eV (dotted line); $\gamma = 0.2$ eV (dashed line); $\gamma = 0.3$ eV (dotted + dashed) and $\gamma = 0.4$ eV (double dotted + dashed). $\varepsilon_r \in [2b - 0.02, 2b + 0.02]$ eV (left panel); $\varepsilon_r \in [2b - 0.04, 2b + 0.04]$ eV (middle panel); $\varepsilon_r \in [2b - 0.1, 2b + 0.1]$ eV (right panel).

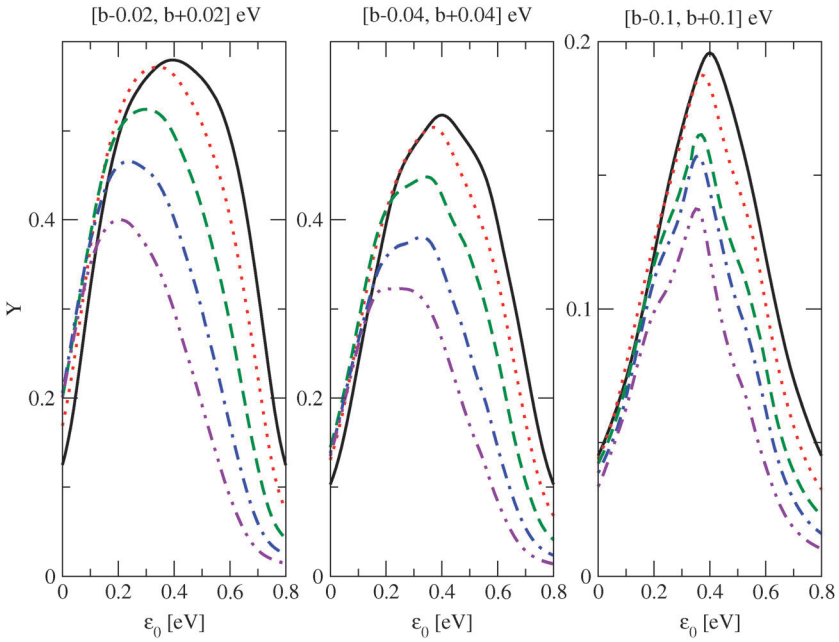

Fig. 7 Yield Y of charge separation as a function of ε_0 obtained with different γ and random parameters b_r for the 29 couplings between the neighbor sites (from site 16 to site 45) for acceptor. $N = 60$, $\eta = 0.05$ eV, $b = 0.2$ eV, $m = 0.1$ eV. $\gamma = 0$ (black line); $\gamma = 0.1$ eV (dotted line); $\gamma = 0.2$ eV (dashed line); $\gamma = 0.3$ eV (dotted + dashed) and $\gamma = 0.4$ eV (double dotted + dashed). $b_r \in [b - 0.02, b + 0.02]$ eV (left panel); $b_r \in [b - 0.04, b + 0.04]$ eV (middle panel); $b_r \in [b - 0.1, b + 0.1]$ eV (right panel).

The peak values of the line shape decrease as the random distribution broadens. In Fig. 6 this is because as the energy gap from D to site 1 increases, the tunneling becomes more difficult as the effective acceptor band density starts to drop, due to the disorder. In Fig. 7 the random tunneling parameters make the transfer ineffective, a foreshadowing of Anderson localization that again increases as the distribution broadens.

Although the external random energies added to the 30 sites of the D part will break the symmetry, after an average over 20 realizations we can see the approximate symmetry of the line shape with $\gamma = 0$ in Fig. 6. An exact symmetry of the line shape would be recovered only in an average over many realizations. The lineshape structures in Fig. 6 and 7 reflect the random site energies. They appear mostly when these site energies are selected from a broad random distribution and depend on the particular realization of this distribution.

VIII. Conclusion

The morphology/geometry of BHJ systems is poorly understood, and therefore a plethora of models has been applied to understand the transport and the overall functioning of these devices. Here we have used a very simple model to examine the effects of acceptor bandwidth, injection energy gaps, coulomb binding and disorder in the acceptor band. The model assumes one-dimensional tight-binding electronic behavior, and a sharp D/A interface. By installing a self-energy term at site N we can use an $N + 1$ site system to represent the organic system plus accepting electrode. The A^- population on the acceptor sites can decay by tunneling into the electrode, or can recombine with D^+, decaying back to the ground state. The yield is simply the fraction of electrons to reach the electrode. If the injection energy gap lies outside the band, the localized population cannot tunnel, and must decay by recombination. Therefore, too large a "LUMO–LUMO gap" should show low quantum efficiency. For the population inside the band, the two decay processes compete. The yield increases with interface D/A electronic coupling, but decreases with stronger D^+A^- coulomb attraction and with the tunneling recombination amplitude. The charge trapping induces a shift of the yield line shape, and the yield drops even for a small energy gap due to the coulomb binding. The exoergicity ε_0 of the charge separation $D^*A \rightarrow D^+A^-$, usually referred to as the LUMO–LUMO gap, generally provides enough energy for the charge separation process to overcome the D^+A^- coulomb attraction. If the D^+ energy ε_0 is too small, then the recombination will occur and few electrons are injected. If it is too large the A bandwidth cannot accommodate the exoergicity (there are no resonant states) and very small yield is seen. This is bit counterintuitive since larger energy gaps would seem to favor injection due to better charge separation, but it follows directly from considerations of state densities. Optimal injection occurs for the gap $0 < \varepsilon_0 < 4b$, where $4b$ is the bandwidth. Randomness in the site energies or intersite tunneling makes the transfer less effective, with a lower yield.

Acknowledgements

This work was supported by the Non-Equilibrium Energy Research Center (NERC) which is an Energy Frontier Research Center funded by the U.S. Department of Energy, Office of Science, Office of Basic Energy Sciences under Award Number DE-SC0000989. The research of A. N. is supported by the Israel Science Foundation Grant No. 1646/08, the U.S.-Israel Binational Science Foundation, the Germany–Israel Foundation, and the European Research Commission. MR thanks the NSF for support (CHE-1058896).

References

1 B. Kippelen and J. L. Brédas, *Energy Environ. Sci.*, 2009, **2**, 251.
2 S. Gunes, H. Neugebauer and N. S. Sariciftci, *Chem. Rev.*, 2007, **107**, 1324.
3 J. D. Servaites, S. Yeganeh, M. A. Ratner and T. J. Marks, *Adv. Funct. Mater.*, 2010, **20**, 97.
4 C. W. Tang, *Appl. Phys. Lett.*, 1986, **48**, 183.
5 K. M. Coakley and M. D. McGehee, *Chem. Mater.*, 2004, **16**, 4533.
6 G. Dennler, M. C. Scharber and C. J. Brabec, *Adv. Mater.*, 2009, **21**, 1.
7 J. L. Brédas, J. Cornil and A. J. Heeger, *Adv. Mater.*, 1996, **8**, 447.
8 T. M. Clarke and J. R. Durrant, *Chem. Rev.*, 2010, **110**, 6736.
9 B. C. Thompson and J. M. J. Fréchet, *Angew. Chem., Int. Ed.*, 2008, **47**, 58.
10 J. Lee, *et al.*, *J. Am. Chem. Soc.*, 2010, **132**, 11878.
11 D. Veldman, *et al.*, *J. Am. Chem. Soc.*, 2008, **130**, 7721.
12 I.-W. Hwang, D. Moses and A. J. Heeger, *J. Phys. Chem. C*, 2008, **112**, 4350.
13 N. S. Lewis, *Science*, 2007, **315**, 798.
14 Y. Liang, *et al.*, *J. Am. Chem. Soc.*, 2009, **131**, 7792.
15 S. H. Park, *et al.*, *Nat. Photonics*, 2009, **3**, 297.
16 J. Peet, *et al.*, *Nat. Mater.*, 2007, **6**, 497.
17 R. B. Ross, *et al.*, *Nat. Mater.*, 2009, **8**, 208.
18 R. Kroon, *et al.*, *Polym. Rev.*, 2008, **48**, 531.
19 L. X. Chen, S. Q. Xiao and L. P. Yu, *J. Phys. Chem. B*, 2006, **110**, 11730.
20 J. C. Guo, *et al.*, *New J. Chem.*, 2009, **33**, 1497.
21 A. Datta and S. K. Pati, *Chem. Soc. Rev.*, 2006, **35**, 1305.
22 A. Datta, F. Terenziani and A. Painelli, *ChemPhysChem*, 2006, **7**, 2168.
23 J. F. Rabek, *Photochemistry and Photophysics*, CRC, Florida, 1991.
24 M. Scharber, *et al.*, *Adv. Mater.*, 2006, **18**, 789.
25 B. P. Rand, D. P. Burk and S. R. Forrest, *Phys. Rev. B: Condens. Matter Mater. Phys.*, 2007, **75**, 115327.
26 X. Y. Zhu, Q. Yang and M. Muntwiler, *Acc. Chem. Res.*, 2009, **42**, 1779.
27 M. G. Reuter, T. Hansen, T. Seideman and M. A. Ratner, *J. Phys. Chem. A*, 2009, **113**, 4665.
28 V. Ben-Moshe, A. Nitzan, S. S. Skourtis and D. N. Beratan, *J. Phys. Chem. C*, 2010, **114**, 8005.
29 V. Ben-Moshe, D. Rai, S. S. Skourtis and A. Nitzan, *J. Chem. Phys.*, 2010, **133**, 054105.
30 D. Rai, O. Hod and A. Nitzan, *J. Phys. Chem. C*, 2010, **114**, 20583.
31 D. Rai, O. Hod and A. Nitzan, *J. Phys. Chem. Lett.*, 2011, **2**, 2118.
32 A. Nitzan, *Chemical Dynamics in Condensed Phases*, Oxford University Press, Oxford, 2006.
33 G. C. Solomon, D. Q. Andrews, R. P. Van Duyne and M. A. Ratner, *Phys. Chem. Chem. Phys.*, 2009, **10**, 257.